Available online at www.sciencedirect.com
ScienceDirect
International Journal of Multiphase Flow 33 (2007) 1271–1283
International Journal of Multiphase Flow
www.elsevier.com/locate/ijmulflow

Single-phase convection and boiling heat transfer: Confined single and array-circular impinging jets

Seong-Je Wu [1], Chang Hwan Shin [2], Kyung Min Kim, Hyung Hee Cho *

Department of Mechanical Engineering, Yonsei University, Seoul 120-749, Republic of Korea

Received 19 December 2006; received in revised form 1 June 2007

Abstract

In the present study, the effects of diverse situations of confinement on heat transfer from single and array-circular jet impingements are carefully investigated over various heat transfer regimes of single-phase convection and fully developed nucleate boiling. For the single, circular, unconfined free-surface jet, the transition to turbulence was observed to start around $x/d = 5.5$ and end around $x/d = 9$. For the array-circular jet, however, the wall jet structure yielded no transition to turbulence for all the tested cases, instead monotonically decreasing the convection coefficient. Conversely, the single-circular jet experienced the transition for $V \geqslant 6.1$ m/s. For the confined submerged jet, the transition length was very short due to the vigorous mixing driven by lateral velocity components, and the locus of the secondary peak moved downstream as velocity increased. The temperature distributions of the confined array-circular jet were fairly uniform over the whole heated surface. The averaged single-phase convection coefficients indicated that the confined jet provided the most uniform convection in the lateral direction.

Keywords: Convective boiling; Heat transfer; Impinging jet; Liquid jet; Two-phase flow

1. Introduction

The impinging jet has been regarded as a solution to critical cooling requirements, particularly in cases where very high rates of heat removal are necessary. Jet impingement cooling is employed in numerous industrial applications such as annealing of hot steal sheets, cooling of electronic devices gas turbine blades, and so forth. The limited range of the cooling capacity spectrum afforded by air jet impingement is extended by employing liquid jets that, by convective nucleate boiling, yield higher cooling performance. Jet impingement enhances the convective heat transfer coefficient in the nucleate boiling regime and increases the CHF, or maximum heat flux, thereby extending the wall superheat range of stable operating conditions.

* Corresponding author. Tel.: +82 2 2123 2828; fax: +82 2 312 2159.
E-mail address: hhcho@yonsei.ac.kr (H.H. Cho).
[1] Present address: Samsung Electronics Inc., Kyungki-do, Republic of Korea.
[2] Present address: Korea Atomic Energy Research Institute, Daejeon, Republic of Korea.

0301-9322/$ - see front matter © 2007 Elsevier Ltd. All rights reserved.
doi:10.1016/j.ijmultiphaseflow.2007.06.005

Both air and liquid jet impingements have been applied to electronics cooling applications. In 1983, IBM shipped its first system using array jets that cooled the 64 mm by 64 mm multi-chip module used in the IBM 4381 processor containing 36 chips with a direct thermal path from the back of each chip to the ceramic cap via thermal paste. This cooling scheme (Chu, 1998, 1999) employed so-called highly parallel impingement. A liquid array-jet impingement cooling system using fluorocarbon (Ing et al., 1993) was utilized in the SSI supercomputer SS-1 to dissipate 40 W on 6.5 mm chips.

Confinement is inevitable in many applications of impinging jets due to spatial claims or installation limitations. Jet confinement in the stagnation and/or wall jet region(s) may alter the flow field and heat transfer to be different from those of the unconfined jet as reviewed by Garimella (2000). Such is also the case when heat transfer augmentation techniques are imposed on the target surface, thus necessitating a thermal analysis that considers the degree of confinement. The confinement of liquid jets arises even more diverse situations than that of air jets. Moreover, jet impingement boiling can be seriously deteriorated by confinement due to considerable volumetric expansion by phase change, which increases the size of the pressure drop and can decrease the maximum heat flux.

Despite the importance of considering confinement in the design of liquid jet impingement cooling systems, there has been little study of confined liquid impinging jets. The partial boiling regime is another topic that has received less attention than its usefulness would dictate. This regime has been regarded as a transition from single-phase convection to fully developed nucleate boiling. However, the high convection of jet impingement commonly prolongs the heat flux range where partial boiling is available. Partial boiling of a water jet may cover a heat flux range of 30–300 W/cm^2, which corresponds to the heat generation densities of many industrial applications where jet impingement boiling can be applied as an effective cooling method. Therefore, in the present study, the effects of confinement on jet impingement heat transfer are carefully investigated over the various heat transfer regimes of single-phase convection, partial boiling and fully developed nucleate boiling.

Myriad studies of heat transfer from liquid jet impingement have been conducted for single-phase convection, nucleate boiling and CHF. The high transport of jet impingement substantially extends the heat flux range corresponding to the partial boiling regime, thus covering the diversity of the heat removal rates required in industrial applications. Although there exists great potential for applying partial boiling to cooling applications, few investigations of the matter have been reported in the open literatures. To date, Vader, Wolf and their coworkers (Vader et al., 1992; Wolf et al., 1993, 1996) have been the only individuals to date to conduct and report comprehensive investigations of partial boiling. Conversely, the onset of nucleate boiling has attracted the attention of some researchers (Miyasaka and Inada, 1980; Ma and Bergles, 1986; Mudawar and Wadsworth, 1991; Vader et al., 1992), and fully developed nucleate boiling and CHF have been extensively investigated.

Local investigations are essential to understanding the relationship between jet impingement heat transfer and other parameters. For single-phase convection, local measurements of heat transfer are commonly employed as module-averaged ones, but the installation of as many sensors as are required to obtain fine resolution data sets can be difficult when high-heat flux is involved. Heater material in the form of shim stock or thin foil, which is commonly used in local measurements, is too delicate to apply to the high-heat flux conditions associated with nucleate boiling, let alone CHF. Thus, very few of the previous investigations on jet impingement boiling have included local measurements. As for thorough local considerations, to the best of our knowledge, there have been no studies in addition to those of Vader et al. (1992), Wolf et al. (1993 and 1996), and their extensions.

Confined circular jets have a greater confinement effect because of their three-dimensional flow characteristics. In the present study, we investigated single and array-circular subcooled water jets impinged on to a heated surface to explain the local heat transfer of single-phase convection, partial boiling and fully developed boiling; furthermore, we compared the jet impingement heat transfer characteristics of an unconfined free-surface jet and a confined submerged jet.

2. Experimental methods

2.1. Experimental apparatus

A schematic of the test loop is presented in Fig. 1. The main and secondary reservoirs control system temperature and pressure, condense the vaporized coolant, and deaerate the coolant. A magnetic pump circulates

the flow through the loop, and the rotation speed of the magnetic pump is controlled via an inverter. One of three positive-displacement-type flowmeters is used during the experiment according to the flowrate range. A heat exchanger is connected to a constant temperature bath to control the jet temperature. The heat exchanger comprises several annular, two-stream counter flow-type components. Most portions of the piping were insulated to aid in the regulation of flow loop temperature. A bypass and a flow control valve were placed around the magnetic pump and upstream of the test section, respectively, to control the flowrate with the inverter of the pump. Three J-type thermocouples were located directly upstream and downstream of the flowmeters and downstream of the heat exchanger to monitor temperatures through the flow loop.

A schematic of test section employed herein is presented in Fig. 2. To avoid leakages, as many parts as possible were constructed to be cylindrical. The settling chamber (plenum) has just one small baffle. The pressure taps are situated in the settling chamber and downstream of the nozzle and are used to measure the pressure drops between these two positions. In most test cases, the test section was kept open to its surroundings through a hole on its top to ensure the reference pressure in downstream region of the wall jets. This test section was designed to conduct experiments for both the unconfined free-surface jets and confined submerged jets. The impingement surface was placed to be independent of the exit of the test section. Thus, as the wall jets fall off the impingement surface into the pool, the jet flows are not influenced by conditions downstream of the test section. A thermocouple probe installed in this chamber reads the jet temperature. The origin of the coordinate system is the center point of the stagnation line, and the x, y and z coordinates indicate the stream, vertical and lateral directions, respectively.

The DC power supply was connected to the bus bar soldered to the heater at the center of the impingement surface. The heater is made of INCONEL alloy 600 that is 0.467 mm thick, 14.0 mm wide and 140 mm long; however, only an 80 mm portion of the central region is heated, and the distance between the voltage taps used to measure the voltage decrement through the heater is 72 mm. The confined nozzle plate is 15.0 mm wide, which is slightly wider than the heater width. Therefore, despite the top surface of the heater being completely wet with water, moisture is not able to seep underneath the sidewalls of the confined nozzle plate and potentially overheat the heater edge to burnout.

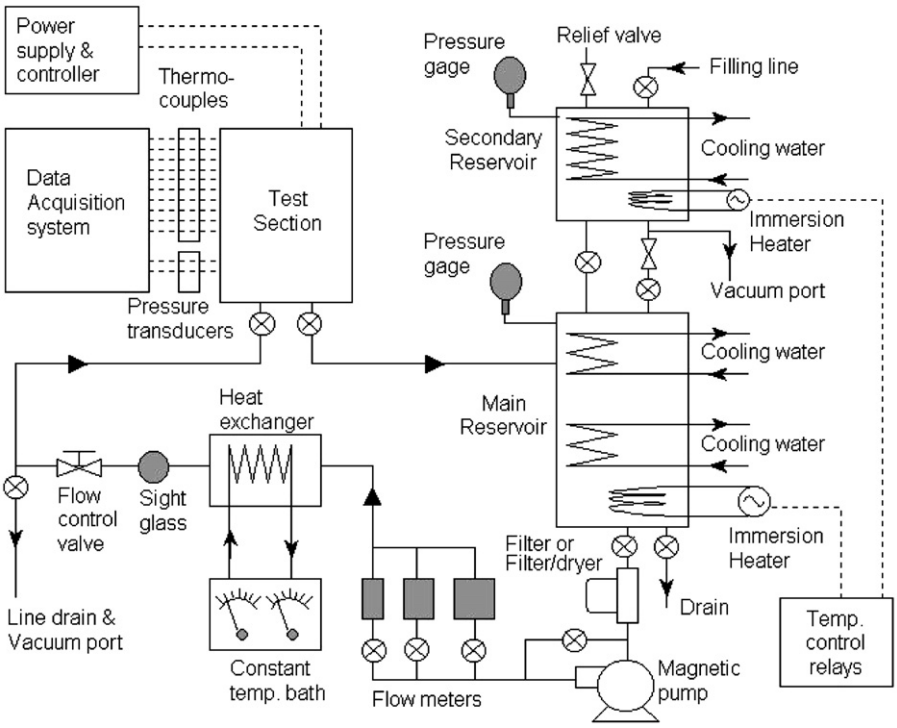

Fig. 1. Schematic of experimental setup.

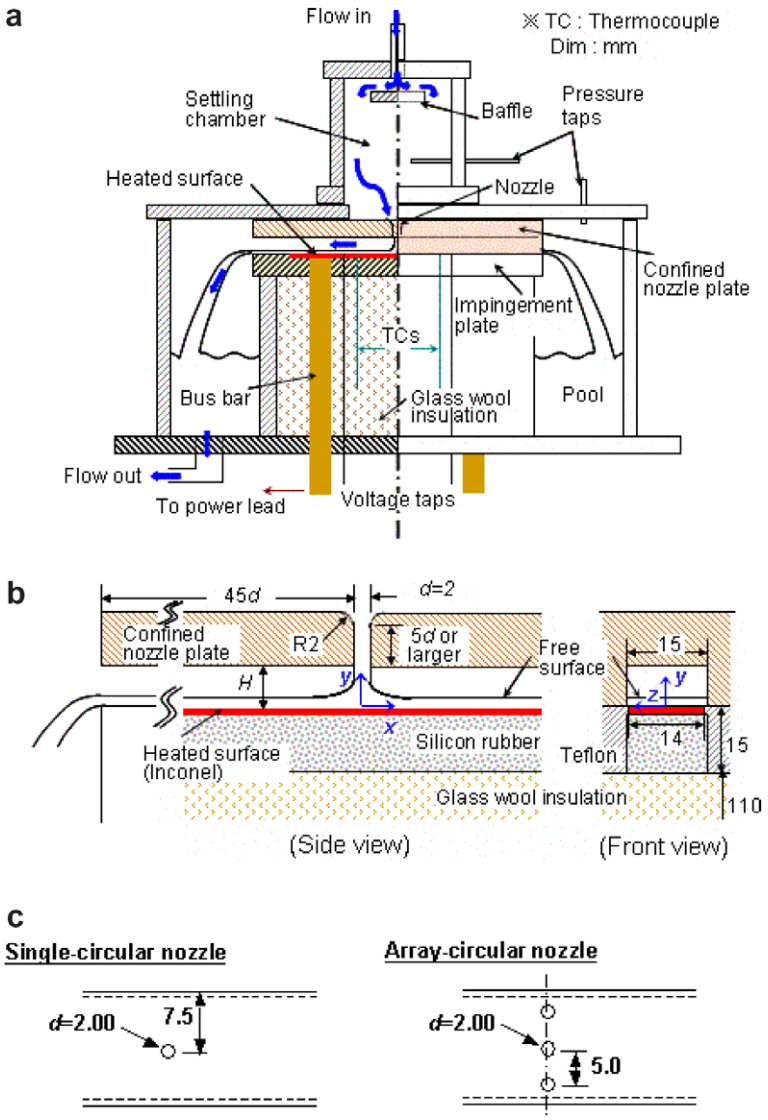

Fig. 2. Schematic of test section. (a) Test section; (b) cross-section view; (c) confined nozzle plate.

Forty-eight K-type thermocouples constructed from 0.127-mm-diameter wires (nickel–chromium and nickel–aluminum, 36-gage, Omega Engineering, USA) were welded to the back side (dry side) of the heater along the centerline, $z/d = 0.0$, and the offset line, $z/d = 2.5$, in the stream direction. The spatial resolution of the heat transfer measurements ranged from 0.5 to 1 nozzle dimension. Three couples of voltage taps were also welded near the soldered bus bars. The welded thermocouple wires and the voltage taps were fixed on the dry side by a high temperature steel epoxy. To keep this side dry, silicon rubber was poured and cured as a sealant and 110-mm-thick glass wool insulation was filled to minimize the heat loss to the dry side. All but the heated surface of the 180 mm × 180 mm impingement plate was constructed of Teflon.

The confined nozzle plate literally confines the flow within a small channel, the height of which is H (spacing between nozzle and heated surface). Depending on the value of H and the flow condition, the wall jet may or may not maintain free surface. The 68-mm-long central region of the nozzle plate maintains a gap of H and a constant outsite gap height of 8 mm. In addition to preventing excessive stagnation pressure that can damage the thin-plate heater module, these dimensions help to maintain a constantly static pressure over the unheated downstream region, which aids in the measurement of downstream static pressure. The confined

nozzle plates provide various nozzle configurations by replacing nozzle inserts with single-circular and in-lined array-circular jets. The single- or array-circular jets have the hole dimension, $d = 2.00$ mm. Since the lengths of the straightening section of the nozzles, ls, are larger than 10 mm, the ratios, ls/d fall into the range from 5 to 17.5. Wadsworth and Mudawar (1990) investigated the effects of nozzle shape for the contoured, V-shape, and flat nozzle inlets. They indicated that the straightening section of 5d provided uniform flow into the impingement region regardless of the nozzle inlet geometry, as well as nearly identical heat transfer. Following these results, the nozzle length employed herein may be considered adequately long for the avoidance of behavioral variations. The coolant was deionized water that was deaerated prior to experimental runs. The data acquisition system comprised a data logger (Agilent Technologies 34970A) and a PC.

2.2. Experimental conditions and data reduction

The circular water jets were examined with the degree of subcooling (ΔT_{sub}, $T_{sat} - T_f$) of 50 °C and the corresponding average coolant temperature at nozzle exit, $T_f = 50$ °C (where T_{sat} is saturation temperature). Both the bulk velocity at nozzle exit (V) and volumetric flow rate (Q) conditions were considered. For the largest H/d, the average jet velocity variation in the pre-impingement region caused by the gravitational acceleration

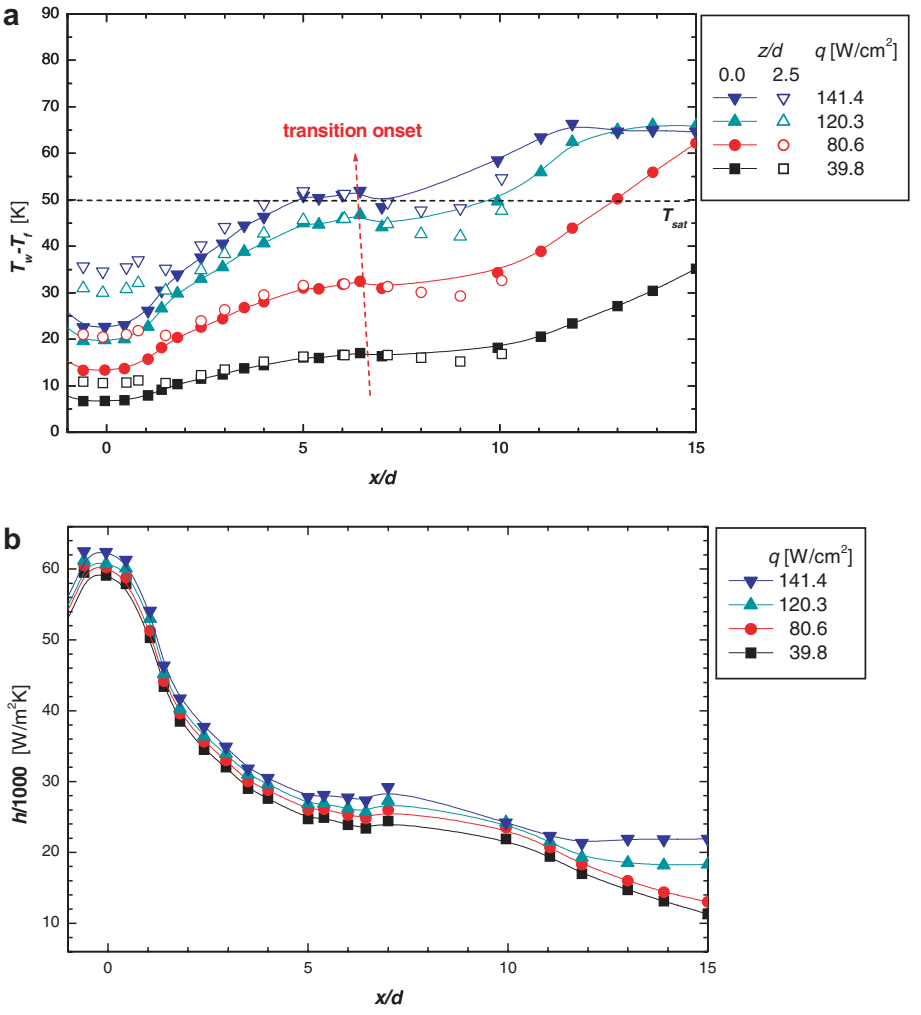

Fig. 3. Temperature and convection coefficient distributions for the unconfined free-surface single-circular jet at $H/d = 5.3$ and $V = 6.1$ m/s ($Q = 1.2$ l/min). (a) Temperature distributions; (b) convection coefficient distributions at $z/d = 0.0$.

was negligible. The test section was kept open to its surroundings through a hole on its top to ensure static, atmospheric pressure downstream of the wall jets regardless of any system pressures. Heat flux covered the single-phase convection and partial nucleate boiling, and reached the fully developed nucleate boiling regimes. The local temperatures measured from the thermocouples welded to the backside of the heater were converted to the wall temperatures of the wetted surface assuming a one-dimensional conduction in the y direction. Based on the analysis of a heater similar in thickness and thermal properties to that employed herein, Wolf (1993) suggested that a two-dimensional finite control volume approach, as opposed to a one-dimensional conduction approach, was indicative of a temperature difference of less than 0.23 °C.

The uncertainly analysis of the experimental measurements in this study was performed following Kline and McClintock (1953) and all errors were estimated with a confidence level of 95%. The calculated error of the main variables revealed the uncertainty of ±1.7 °C for local wall temperature on the target surface (T_w); 3.5% for heat flux with 0.5% heat loss by radiation and conduction; 7.6% for the convection coefficient ($h, q/(T_w - T_f)$); 1.3 % for the average velocity at the nozzle exit (V); 2.9% for the Reynolds number (Re).

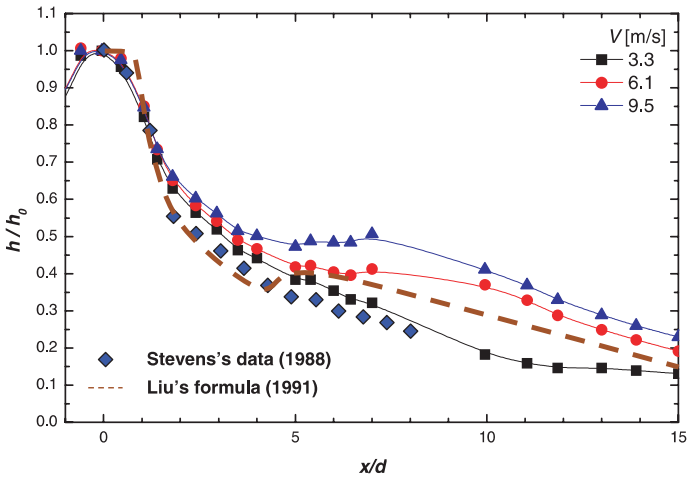

Fig. 4. Velocity effects on normalized single-phase convection coefficient distributions for the unconfined free-surface single-circular jet at $H/d = 5.3$ and $z/d = 0.0$.

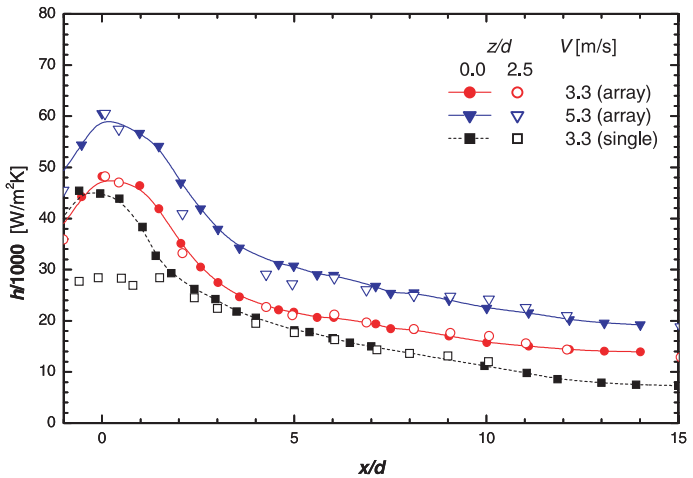

Fig. 5. Single-phase convection coefficient distributions for the unconfined free-surface circular jets at $H/d = 5.3$.

3. Results and discussion

3.1. Unconfined free-surface jets

The wall temperature and convection coefficient distributions for the unconfined free-surface single-circular jet at $H/d = 5.3$ and $V = 6.1$ m/s ($Q = 1.2$ l/min) are plotted in Fig. 3. The small H/d jet with high velocity sometimes results that the wall jet hits the jet nozzle; therefore, the nozzle-to-surface distance of $H/d = 5.3$ was selected instead of $H/d = 1.0$, the reference spacing in the confined jet condition known to sustain a stable free surface because moderate changes to the H/d of free-surface jets do not affect heat transfer. As shown in Fig. 3, the transition region by the jet flow was observed to start from around $x/d = 5.5$ and end around $x/d = 9$. Boiling incipience occurred as far downstream as usual, and as boiling developed, the flat distribution appeared at heat flux (q) of 141 W/cm^2.

Fig. 4 shows the effects of velocity on the normalized single-phase convection coefficient (h/h_0 where h_0 is convection coefficient at stagnation) distributions and provides comparisons of the formula calculated by Liu et al. (1991) and the experimental data reported by Stevens (1988) in case with $H/d = 2.23$, $Re = 10{,}600$ and $q = 10.9$ W/cm^2. The present values agree well with their experimental and formula. The

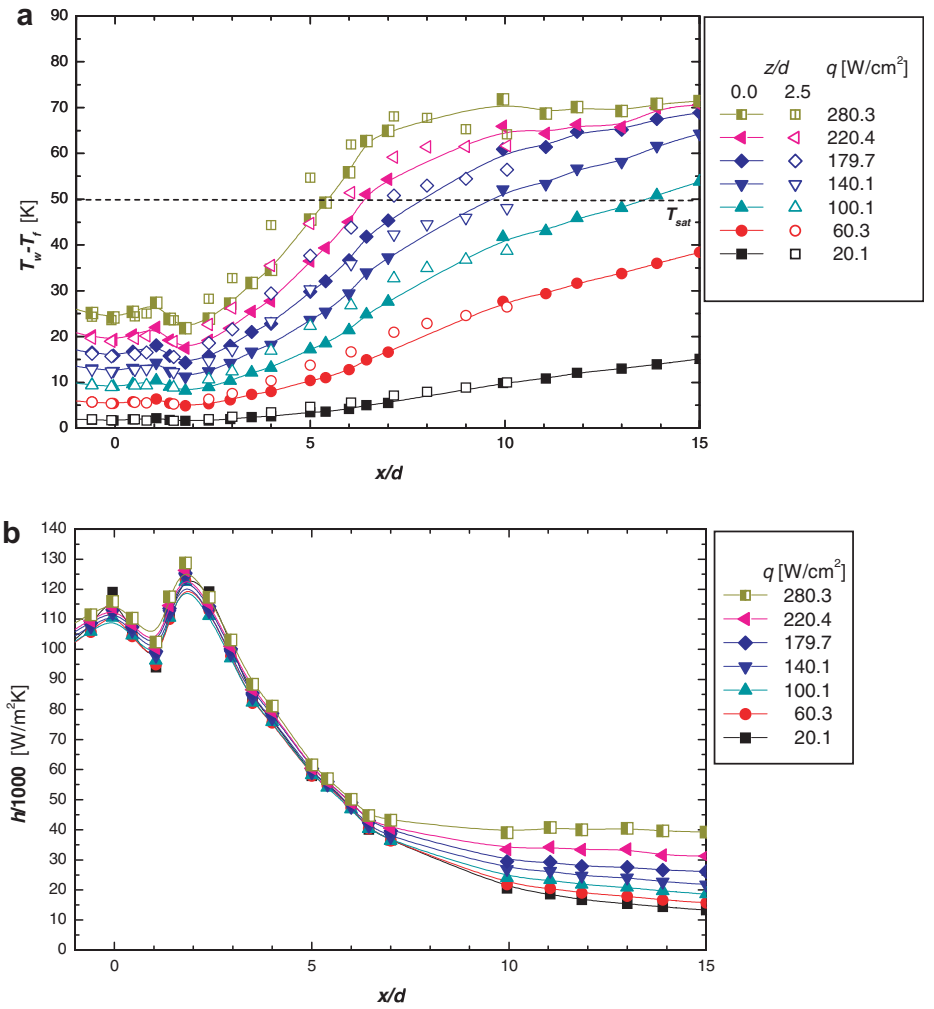

Fig. 6. Temperature and convection coefficient distributions for the confined submerged single-circular jet at $H/d = 1$ and $V = 16.2$ m/s ($Q = 3.0$ l/min) and $z/d = 0.0$. (a) Temperature distributions; (b) convection coefficient distributions at $z/d = 0.0$.

locus of the secondary peak affected by the transition to turbulence was seen at the smaller x/d with increasing velocity. No hydraulic jump took place in the heated region as the measured $r_{jump}/d > 12$ (where the r_{jump} is location of hydraulic jump for a free-surface circular jet) and also calculated using the empirical correlation (Stevens and Webb, 1991). Thus the transition was not related to the hydraulic jump.

The in-lined array-circular jet, the results of which are presented in Fig. 5, produced a planar, jet-like structure in the wall jet region. This wall jet structure yielded no transition to turbulence for all the tested cases, instead providing monotonic decreases to the convection coefficient, while the singular circular jet experienced transition for $V \geqslant 6.1$ m/s. The flowrate for the array jets was thrice that of the single jet and the mixing of three jets in the wall jet region promoted convection. As such, at an identical velocity, $V = 3.3$ m/s, the convection coefficients were higher for the array jets than for the single jet. Additionally, compared to the single jet, the array jets created a wider plateau around the stagnation region and sustained a gentler decrease in the wall jet region. Since the outer array jets were impinged onto the surface at $z/d = \pm 2.5$, the convection coefficient distributions at the offset line showed good agreement with those at the centerline, which was not the case for the single jet.

3.2. Confined submerged jets

As this study employed channel-type confinement, the circular jet impingement at the high nozzle-to-surface distance of $H/d = 4$ wetted all the confining walls to form a submerged jet due to its strong lateral velocity components. As the average velocity in the confined channel flow decreases with increasing H/d, the confined circular submerged jets were tested for $H/d \leqslant 1$. The temperature and convection coefficient distributions for the confined single-circular jet at $H/d = 1$ and $V = 16.2$ m/s ($Q = 3.0$ l/min) are presented in Fig. 6. Vigorous mixing driven by the lateral velocity components precipitates the transition to turbulence and yields a secondary peak in the convection coefficient around $x/d = 2$ and a very short transition region with a length of about $1d$. Even the magnitude of the secondary peak in Fig. 6b was larger than the stagnation value. The stagnation temperatures at the offset line, $z/d = 2.5$ in Fig. 6a, differed little from those at the centerline, which was not the case with the unconfined free-surface single-circular jet. But due to the stronger momentum along the centerline after the transition, the centerline temperature curves were considerably lower than those of the offset line. As for boiling, which was initiated furthest downstream, the temperature and convection coefficient distributions became constant. The convection coefficients in $x/d < 2.5$ exceeded those of $x/d = 15$ by more than ten times, with an associated temperature difference of 45 °C. As shown in Fig. 7, the more pronounced secondary peak was obtained with increasing velocity. The locus of secondary peak moved downstream as

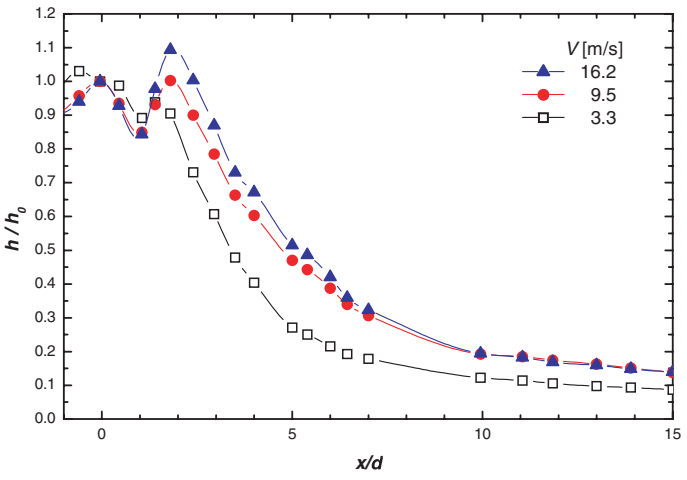

Fig. 7. Velocity effects on normalized single-phase convection coefficient distributions for the confined submerged single-circular jet at $H/d = 1$ and $z/d = 0.0$.

velocity increased, thereby improving the effectiveness of convection over most of the heated surface. For all the tested cases, the stagnation convection coefficient was 7–10-folds that of the case furthest downstream.

The convection coefficient distributions for the confined array-circular jet at $H/d = 1$ and $V = 5.3$ m/s ($Q = 3.0$ l/min) are presented in Fig. 8. The similar mechanism of vigorous mixing by the lateral velocity components promoted the transition to turbulence and yielded an associated apparent secondary peak around $x/d = 1.5$. The lateral temperature distributions were fairly uniform over the whole heated surface, with similar distributions at the centerline and the offset line. The smaller nozzle exit velocity was associated with a flowrate identical to that of the single-circular jet: at $Q = 3.0$ l/min, $V = 5.3$ m/s for the array jets and $V = 16.2$ m/s for the single jet. Thus stagnation to the furthest downstream convection coefficient ratio was reduced to less than 5, as shown in Fig. 9, and the developed boiling region was widened such that $q \geqslant 220$ W/cm^2. As with the single-circular jet, the secondary peak was more pronounced and moved downstream with increasing velocity. As shown in Fig. 9, the velocity effects diminished downstream, such that $x/d > 10$ at $q = 140$ W/cm^2 as boiling was developed.

The boiling curves of the single-circular jets and the array-circular, the general characteristics of which were similar, are plotted in Fig. 10. The dotted line in this Fig. 10 is represented the saturation temperature (T_{sat}) at atmospheric pressure. Due to the large difference in convection between the upstream and downstream

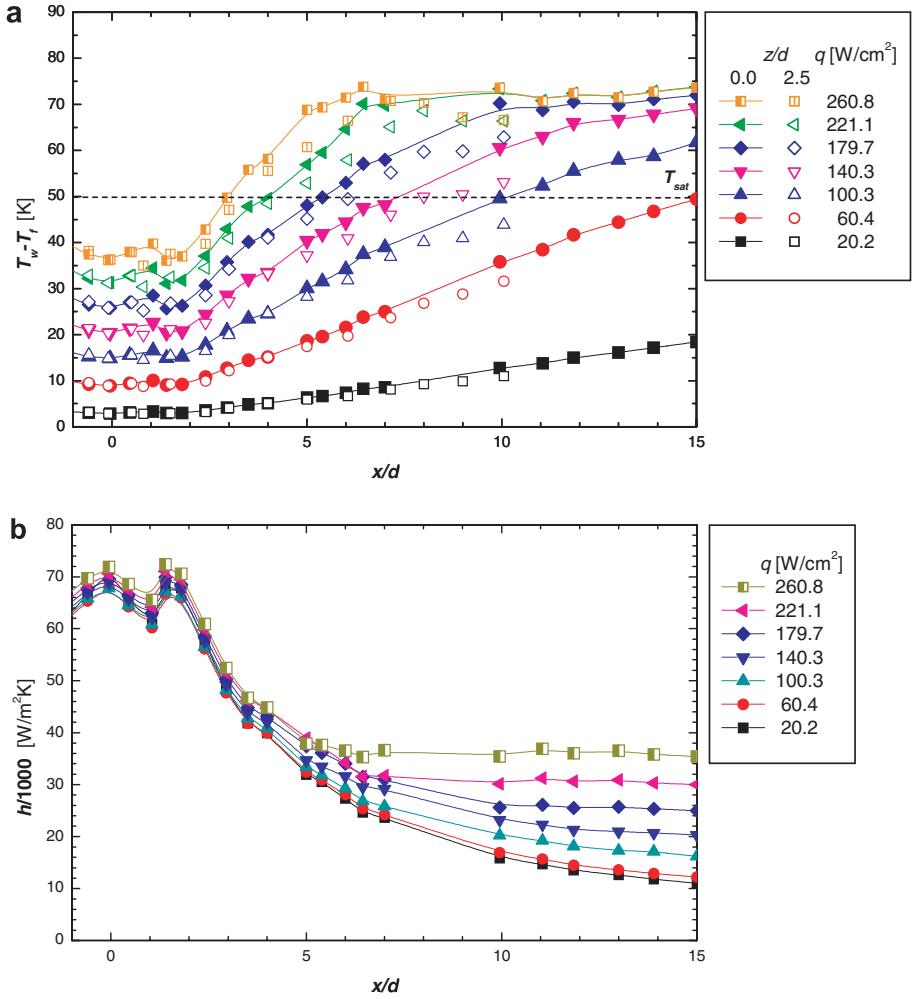

Fig. 8. Temperature and convection coefficient distributions for the confined submerged array-circular jet at $H/d = 1$ and $V = 5.3$ m/s ($Q = 3.0$ l/min) and $z/d = 0.0$. (a) Temperature distributions; (b) convection coefficient distributions at $z/d = 0.0$.

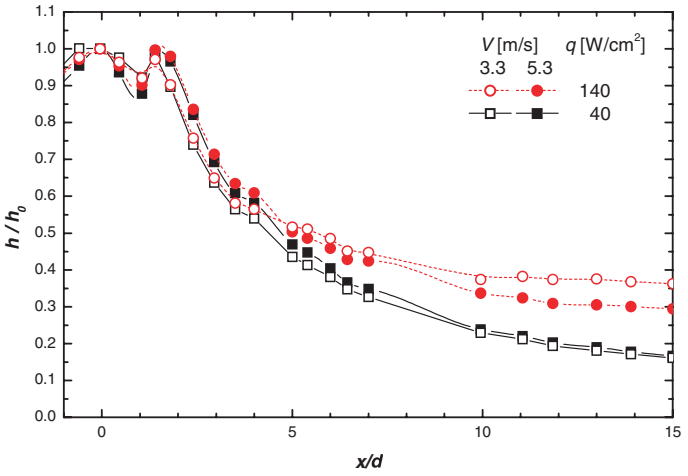

Fig. 9. Velocity effects on normalized convection coefficient distributions for the confined submerged array-circular jet at $H/d = 1$ and $z/d = 0.0$ (single-phase convection at $q = 40$ W/cm^2).

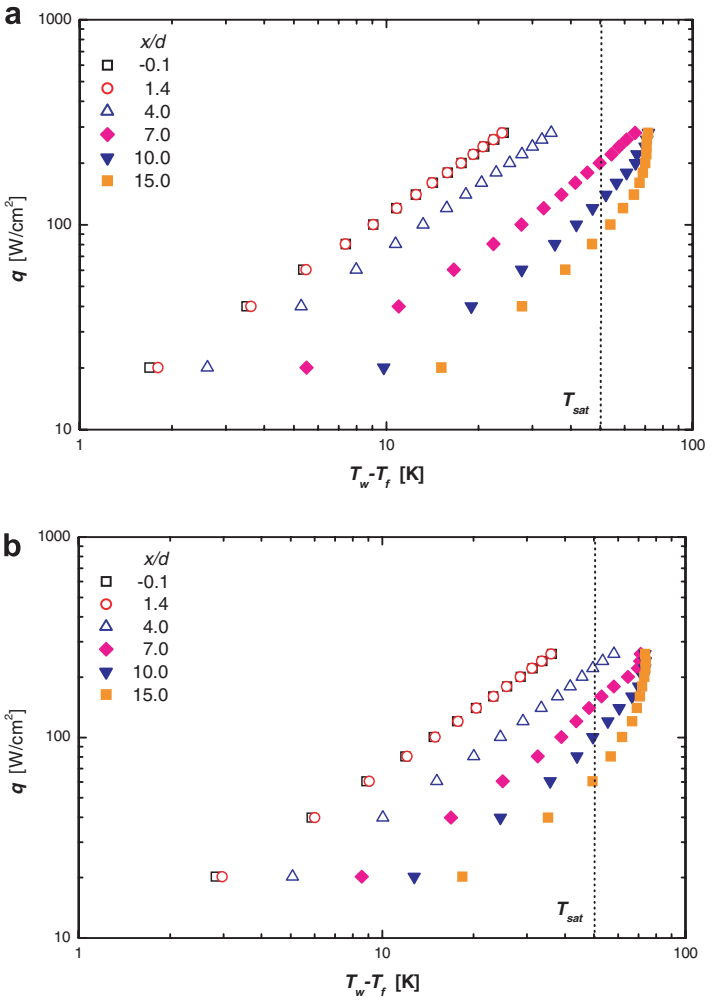

Fig. 10. Boiling curves for the confined submerged circular jet at $H/d = 1$, $Q = 3.0$ l/min, and $z/d = 0.0$. (a) Single-circular jet at $V = 16.2$ m/s; (b) array-circular jet at $V = 5.3$ m/s.

regions, the curves around the stagnation region did not reach the saturation temperature even at the very high flux near 300 W/cm^2. The quick transition for $x/d \leqslant 2$ yielded nearly identical curves at $x/d = -0.1$ and 1.4. As boiling was developed, all curves merged to a single line.

3.3. Effects of confinement

Comparisons of the convection coefficient distributions of the confined and unconfined single-circular jets are illustrated in Fig. 11. Confining the single-circular jets forces the radial flows to be two-way channel flows, enhances mixing and turbulence, and increases the effective flowrate over the heated surface. The precipitated transition to turbulence elevated convection coefficient distributions for the confined single jet at $x/d < 6$ with $V = 9.5$ m/s and at $x/d < 4$ with $V = 3.3$ m/s, indicating that with increased velocity came the extension of the region where the confined jet outperformed the unconfined jet. Enhancement of the stagnation convection coefficient also increased with increasing velocity, which is attributed to the increase in mixing and turbulence associated with increasing velocity.

The streamwise direction-averaged convection coefficients (the convection coefficients averaged between the stagnation point (0.0) and a measurement point (x) in the streamwise direction, $\bar{h} = \frac{1}{x}\int_0^x h\mathrm{d}x$) for the single and array-circular jets are shown in Fig. 12. The difference between the averaged values increased with increasing

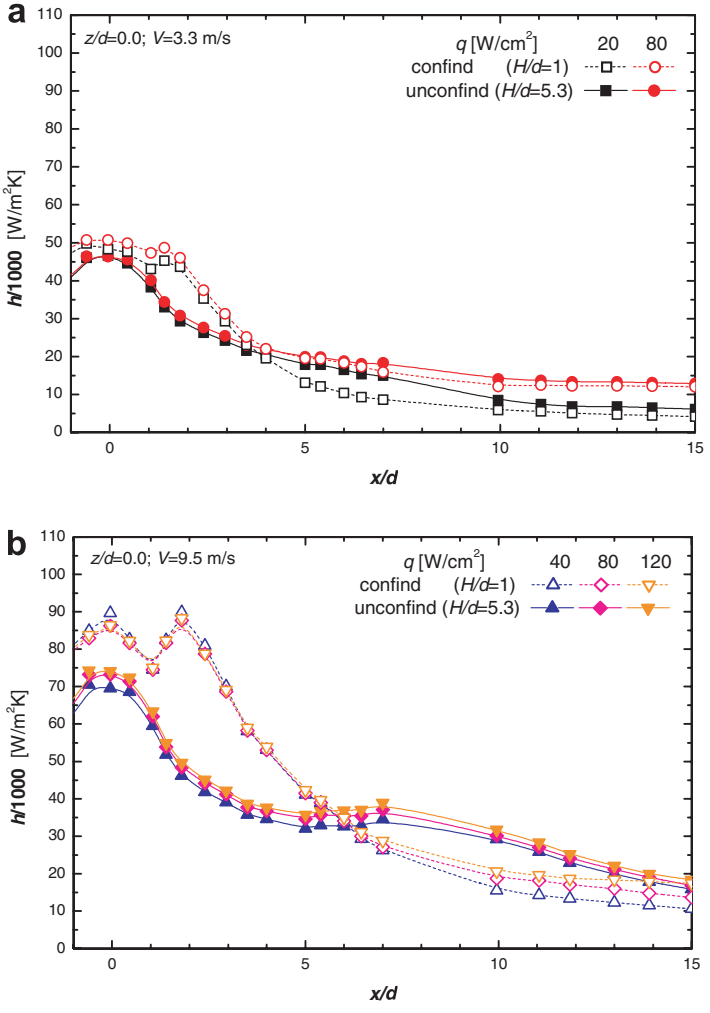

Fig. 11. Effects of confinement on convection coefficient distributions for the single-circular jets at $z = 0.0$. (a) $V = 3.3$ m/s; (b) $V = 9.5$ m/s.

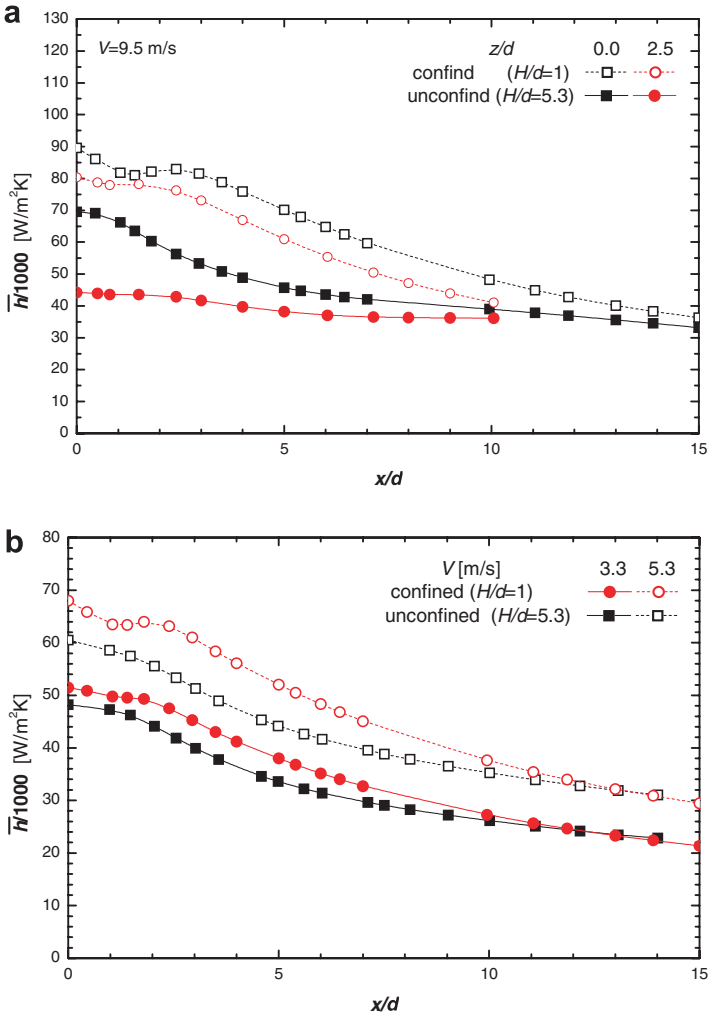

Fig. 12. Effects of confinement on averaged convection coefficient distributions for the single-phase convection. (a) Single jet; (b) array jets.

velocity. The averaged single-phase convection coefficients in Fig. 12a indicate that the confined jet provided more uniform convection in the lateral direction. Thus it is suggested that the channel-type confinement at $H/d \leqslant 1$, imposed on circular jets which are not adequate for cooling of common rectangular heated surfaces, enhances the overall heat transfer and uniformity in the lateral direction. The confined and unconfined array-circular jets are compared in Fig. 12b. As with the single-circular jet, increased mixing and turbulence associated with confinement enhanced the stagnation convection coefficient and caused the transition at $x/d < 2$. It was expected that since the planar jet-like wall jet was associated with the planar jet-like convection coefficient distributions in the free-surface array-circular jet, the confined array-circular jet would provide convection coefficient distributions similar to those for the confined planar jet. However, the results indicated convection coefficient distributions similar to those of the confined single-circular jet. The results contradicted expectation due to significant radial momentum of the outer jets in the array-circular jet. That is, without vigorous mixing and turbulence around the stagnation region, the wall jet region of the confined array-circular jet might maintain characteristics similar to those of the confined planar jet. In addition, confinement provided a stable flowrate over the heated surface. The small number in jet array fostered a three-dimensional flow region distributed across a considerable heated area, thus resulting in the cyclical appearance and disappearance of non-wetted regions far downstream, increasing burnout possibility. Moreover, the momentum loss caused by jet splattering was overcome spontaneously.

4. Conclusions

Comparative investigations were performed for unconfined free-surface and confined submerged jets to examine the effects of confinement on liquid circular and array impinging jets. The regimes of heat transfer of single-phase convection and fully developed nucleate boiling were explored. Confining jet impingement affected heat transfer in various ways depending on system parameters. These effects may be summarized as follows.

For the single-circular unconfined free-surface jet, the transition region by the jet flow was observed to start from around $x/d = 5.5$ and end around $x/d = 9$. The locus of the secondary peak created by the transition to turbulence was seen at the smaller x/d with increasing velocity in the single-phase convection. The in-lined array-circular jet produced a planar jet-like structure in the wall jet. This wall jet structure yielded no transition region for all tested cases, instead providing a monotonic decrease in the convection coefficient, while the single-circular jet experienced a transition for $V \geqslant 6.1$ m/s. The transition region, which occurred over a very short length, was precipitated by vigorous mixing driven by lateral velocity components. The locus of the secondary peak moved downstream as velocity increased in the single-phase convection.

For the confined array jet, the lateral temperature distributions were fairly uniform over the whole heated surface due to similar distributions at the centerline and the offset line. The convection coefficient distributions in the stagnation region of the array-circular jet were similar to those of the confined single-circular jet due to the significant radial momentum of the outer jets in the array-circular jet. That is, without vigorous mixing and turbulence around the stagnation region, the wall jet region of the confined array-circular jet might maintain characteristics similar to those of the confined planar jet. The confining circular jets significantly enhanced mixing and turbulence by forcing the radial flows to be two-way channel flows. Thus the transition to turbulence occurred within $1 \leqslant x/d \leqslant 2$ and the convection coefficients in the stagnation region were enhanced significantly. This channel-type confinement enabled the circular jets to be used more effectively by increasing the actual flowrate over the rectangular heated surface.

References

Chu, R.C., 1998. Advanced cooling technology for leading-edge computer products. In: Proceedings of the Fifth International Conference on Solid-State and Integrated Circuit Technology, Beijing, China, pp. 559–562.

Chu, R.C., 1999. A review of IBM sponsored research and development projects for computer cooling. In: Proceedings of the IEEE 15th Annual Semiconductor Thermal Measurement and Management (SEMI-THERMTM) Symposium, San Diego, USA, pp. 151–165.

Garimella, S.V., 2000. Heat transfer and flow fields in confined jet impingement. Annu. Rev. Heat Transfer 11, 413–494.

Ing, P., Sperry, C., Philstrom, P., Claybaker, P., Webster, J., Cree, R., 1993. SS-1 super computer cooling system. In: Proceedings of IEEE 43rd Electronic Components and Technology Conference, Orlando, FL, USA, pp. 218–237.

Kline, S.J., McClintock, F.A., 1953. Describing uncertainty in single-sample experiments. Mech. Eng. 75, 3–8.

Liu, X., Lienhard, J.H.V., Lombara, J.S., 1991. Convective heat transfer by impingement of circular liquid jets. ASME J. Heat Transfer 113, 571–582.

Ma, C.F., Bergles, A.E., 1986. Jet impingement nucleate boiling. ASME J. Heat Transfer 29, 1095–1101.

Miyasaka, Y., Inada, S., 1980. The effect of pure forced convection on the boiling heat transfer between a two-dimensional subcooled water jet and a heated surface. J. Chem. Eng. Jpn. 13, 22–28.

Mudawar, I., Wadsworth, D.C., 1991. Critical heat flux from a simulated chip to a confined rectangular impinging jet of dielectric liquid. Int. J. Heat Mass Transfer 34, 1465–1479.

Stevens, J., 1988. Measurements of Local Heat Transfer Coefficients: Results for an Axisymmetric, Single-phase Water Jet Impinging Normally on a Flat Plate with Uniform Heat Flux. Master thesis, Brigham Young University, Provo Utah.

Stevens, J., Webb, B.W., 1991. Local heat transfer coefficients under an axisymmetric single-phase liquid jet. ASME J. Heat Transfer 113, 71–78.

Vader, D.T., Incropera, F.P., Viskanta, R., 1992. Convective nucleate boiling on a heated surface cooled by an impinging planar jet of water. ASME J. Heat Transfer 114, 152–160.

Wadsworth, D.C., Mudawar, I., 1990. Cooling of a multichip electronic module by means of confined two-dimensional jets of dielectric liquid. ASME J. Heat Transfer 112, 891–898.

Wolf, D.H., 1993. Turbulent Development in a Free-surface Jet and Impingement Boiling Heat Transfer. Ph.D. Thesis, Purdue University, West Lafayette, IN, USA.

Wolf, D.H., Incropera, F.P., Viskanta, R., 1996. Local jet impingement boiling heat transfer. Int. J. Heat Mass Transfer 39, 1395–1406.